




Spectral gain profile of a multi-stack terahertz quantum cascade laser

Journal Article**Author(s):**

Bachmann, Dominic; Rösch, Markus; Deutsch, Christoph; Krall, Michael; Scaliari, Giacomo ; Beck, Mattias ; Faist, Jérôme 
Unterrainer, Karl; Darmo, Juraj

Publication date:

2014-11-03

Permanent link:

<https://doi.org/10.3929/ethz-b-000093720>

Rights / license:

[Creative Commons Attribution 3.0 Unported](#)

Originally published in:

Applied Physics Letters 105(18), <https://doi.org/10.1063/1.4901316>

Spectral gain profile of a multi-stack terahertz quantum cascade laser

Cite as: Appl. Phys. Lett. **105**, 181118 (2014); <https://doi.org/10.1063/1.4901316>

Submitted: 06 August 2014 . Accepted: 27 October 2014 . Published Online: 07 November 2014

D. Bachmann, M. Rösch, C. Deutsch, M. Krall, G. Scalari, M. Beck, J. Faist, K. Unterrainer, and J. Darmo



View Online



Export Citation



CrossMark

ARTICLES YOU MAY BE INTERESTED IN

[Dispersion in a broadband terahertz quantum cascade laser](#)

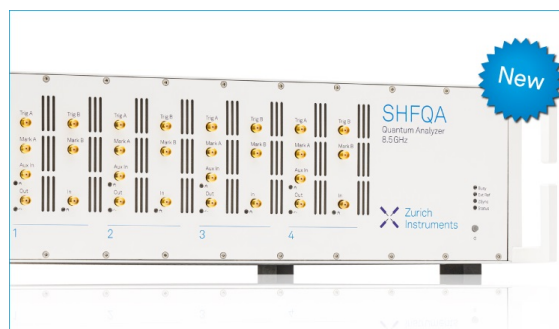
Applied Physics Letters **109**, 221107 (2016); <https://doi.org/10.1063/1.4969065>

[Gain dynamics in a heterogeneous terahertz quantum cascade laser](#)

Applied Physics Letters **113**, 181102 (2018); <https://doi.org/10.1063/1.5049384>

[Thermoelectrically cooled THz quantum cascade laser operating up to 210 K](#)

Applied Physics Letters **115**, 010601 (2019); <https://doi.org/10.1063/1.5110305>



Your Qubits. Measured.

Meet the next generation of quantum analyzers

- Readout for up to 64 qubits
- Operation at up to 8.5 GHz, mixer-calibration-free
- Signal optimization with minimal latency

Find out more



Spectral gain profile of a multi-stack terahertz quantum cascade laser

D. Bachmann,^{1,2,a)} M. Rösch,³ C. Deutsch,^{1,2} M. Krall,^{1,2} G. Scalari,³ M. Beck,³ J. Faist,³ K. Unterrainer,^{1,2} and J. Darmo^{1,2}

¹Photonics Institute, Vienna University of Technology, Gußhausstraße 27-29, 1040 Vienna, Austria

²Center for Micro- and Nanostructures, Vienna University of Technology, Floragasse 7, 1040 Vienna, Austria

³Institute for Quantum Electronics, ETH Zürich, Auguste-Piccard-Hof 1, 8093 Zürich, Switzerland

(Received 6 August 2014; accepted 27 October 2014; published online 7 November 2014)

The spectral gain of a multi-stack terahertz quantum cascade laser, composed of three active regions with emission frequencies centered at 2.3, 2.7, and 3.0 THz, is studied as a function of driving current and temperature using terahertz time-domain spectroscopy. The optical gain associated with the particular quantum cascade stacks clamps at different driving currents and saturates to different values. We attribute these observations to varying pumping efficiencies of the respective upper laser states and to frequency dependent optical losses. The multi-stack active region exhibits a spectral gain full width at half-maximum of 1.1 THz. Bandwidth and spectral position of the measured gain match with the broadband laser emission. As the laser action ceases with increasing operating temperature, the gain at the dominant lasing frequency of 2.65 THz degrades sharply. © 2014 Author(s). All article content, except where otherwise noted, is licensed under a Creative Commons Attribution 3.0 Unported License. [<http://dx.doi.org/10.1063/1.4901316>]

The large variety of applications in the terahertz (THz) frequency range, such as spectroscopy and imaging,¹ triggered strong interest in developing powerful solid-state sources for coherent THz radiation. In terms of size, output power, and efficiency, THz quantum cascade lasers (QCLs)^{2,3} are the devices of choice to generate such radiation. These electrically pumped semiconductor lasers are capable of delivering watt-level output power^{4,5} and reach maximum operating temperatures up to 200 K.⁶ Dependent on the specific application, it is essential to use single mode lasers with high spectral purity, e.g. for local oscillators in heterodyne receivers,⁷ whereas for other applications, THz QCLs with broadband gain media are highly desirable. These range from THz amplifiers for time-domain spectroscopy (TDS)⁸ to tunable external-cavity lasers.⁹ It has been demonstrated that THz QCLs can be actively mode-locked to produce transform limited THz pulses,¹⁰ and very recently, that they can form a frequency comb, if the inherent group velocity dispersion (GVD) is compensated.¹¹ However, all these contributions have in common that they use homogeneous active regions with a rather narrow gain bandwidth, which in the case of Refs. 10 and 11, limits the minimum duration of the mode-locked pulses to ~ 10 ps and the continuously lasing comb bandwidth to ~ 300 GHz. A very promising approach to increase the bandwidth of QCLs is to stack different active regions with individually designed emission frequencies into a single waveguide. This concept of heterogeneous active regions was initially applied to mid-infrared QCLs¹² and later adapted to THz QCLs, where broadband lasing with bandwidths up to ~ 1 THz has been demonstrated.¹³

Such heterogeneous active regions offer high design freedom to shape the optical gain by changing the strength and spectral separation of the individual optical transitions,

as well as the number of cascades and their composition in the waveguide. Because additional requirements, such as identical threshold currents of the different stacks, make the overall design very crucial, THz-TDS gain measurements provide valuable information for bandstructure design and consequently enable further improvement of heterogeneous active regions.^{14,15} Gain measurements of a two-stack THz QCL, processed in a single plasmon waveguide, were presented in Ref. 16. However, these devices show only two color emission.

In this letter, we present a detailed characterization of an ultra-broadband multi-stack THz QCL gain medium, confined in a metal-metal waveguide. We analyze how the spectral gain of the individual stacks develops with bias and temperature and compare the measured intensity gain with the broadband lasing spectrum under the same operating conditions. The near unity confinement of the optical mode and its almost homogeneous field distribution across the entire active region, independent of emission frequency, makes the metal-metal waveguide highly suitable for heterogeneous THz QCLs. In order to overcome the issue of the very low coupling efficiency of the broadband THz pulses into the sub-wavelength metal-metal waveguide, we employ a coupled cavity geometry.^{17,18}

The studied devices were fabricated from a nominally identical quantum cascade design as presented in Ref. 13. The GaAs/Al_{0.15}Ga_{0.85}As heterostructure consists of three active regions, designed for center frequencies at 2.3, 2.7, and 3.0 THz, each grown with 80 periods, yielding a total thickness of 17 μm . Every stack is a rescaled version of a four-quantum well longitudinal optical (LO) phonon depopulation active region.¹⁹ In order to solve the electrical instability issues of this active region (discussed in Ref. 13), the top contact layer and the first stack with 40 periods of the 3.0 THz quantum cascades were removed by reactive ion etching (RIE). The metal-metal resonators of the $39 \times 120 \mu\text{m}$ emitter section and the $1900 \times 120 \mu\text{m}$ QCL

^{a)}Author to whom correspondence should be addressed. Electronic mail: dominic.bachmann@tuwien.ac.at

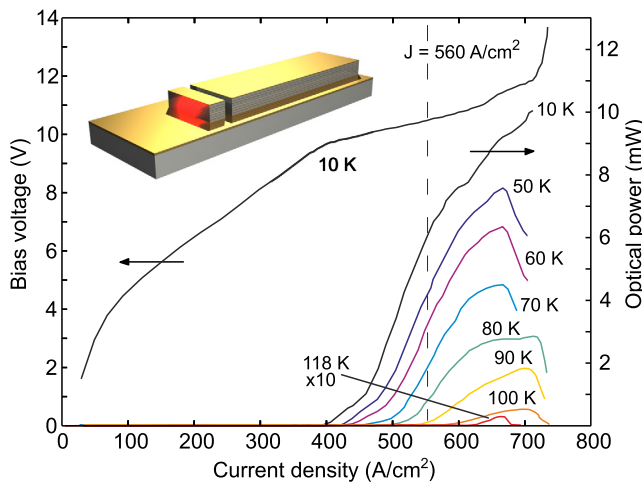


FIG. 1. Current-voltage characteristic at a heat sink temperature of 10 K and temperature dependent light-current characteristics of a coupled cavity device, processed in a metal-metal waveguide. The inset on the left side depicts a coupled cavity device with near-infrared excitation of the THz emitter.

gain section were defined by a dry etching process, self-aligned to the top Ti/Au waveguide layer.²⁰ A 3 μm wide gap between the two sections ensures electrical insulation, and yet maintains a high optical coupling efficiency.¹⁷

Figure 1 shows the temperature dependent light-current-voltage characteristic (LIV) of a typical coupled cavity device. For the sake of consistency of the LIVs with the later presented THz-TDS bias dependent gain measurements, the QCL section and the THz emitter section were synchronously driven with a repetition rate of 10 kHz and a duty cycle of 10%. The QCL section showed lasing up to a heat-sink temperature of 118 K, with a threshold current density of 390 A/cm^2 at 10 K. The commonly used exponential relation $J_{\text{th}}(T) = J_0 + J_1 \exp(T/T_0)$ for the temperature dependence of the threshold current density reveals a characteristic temperature T_0 of 38 K.

Bias and temperature dependent gain measurements of the heterogeneous active region were performed using a standard THz-TDS setup. Near-infrared (NIR) laser pulses, generated by a mode-locked Ti:Sapphire laser (~ 90 fs pulse duration, 801 nm central wavelength, and 80 mW optical power), were used to generate broadband THz pulses by facet excitation of the integrated emitter. The mode of these THz pulses efficiently couples into the gain section and propagates through the metal-metal cavity. The radiation, emitted from the QCL output facet, was collected by a 50 mm off-axis parabolic mirror and focused onto a 1 mm thick ZnTe (110) crystal for electro-optic detection of the THz electric field.

In order to measure only the THz electric field that is modulated by the QCL, and eliminate any radiation which was not propagating through the metal-metal waveguide, a double modulation scheme was used in an $f/2f$ mode.^{14,15} The emitter section was square wave modulated at a repetition rate of 20 kHz and a duty cycle of 20%, whereas the QCL gain section was independently modulated at 10 kHz and a duty cycle of 10%. Due to the missing top contact layer of the active region, the emitter section could be reverse-biased with amplitudes up to -30 V, without driving

a significant dark current through the structure. The detected modulation signal exhibits frequency components up to 3.7 THz and reveals an SNR of 400 at 2.0 THz (not shown). From the transmitted difference signal (QCL on–QCL off) and an additional reference signal (QCL off), the gain was calculated from a 12.2 ps long window, containing the THz pulse passing through the QCL gain section twice.

Figure 2(a) shows the measured intensity gain as a function of frequency at relevant current densities. The insets indicate the particular operating points on the LIV curve. As the applied current is increased towards the laser threshold, the bandstructure of the 2.7 and 3.0 THz stacks start to align and provide gain with the maximum at ~ 2.65 THz. At the threshold current density of 390 A/cm^2 , the gain has a flat top across ~ 500 GHz. Close to the operating point at which the QCL exhibits the largest emission bandwidth (560 A/cm^2), all three stacks experience sufficient gain to initiate lasing and the full width at half-maximum (FWHM) of

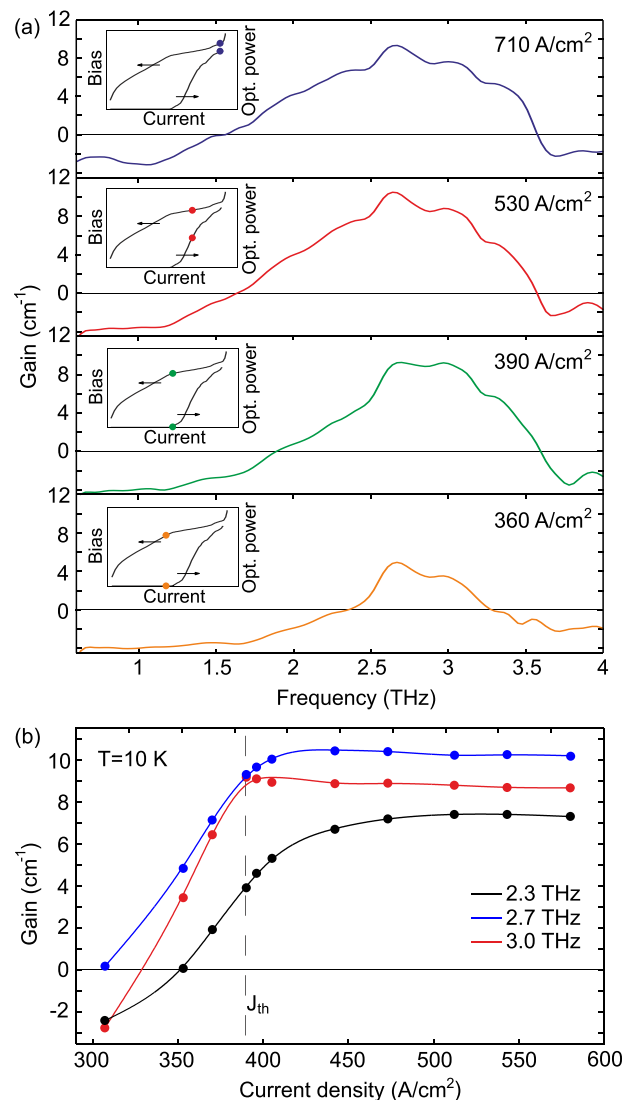


FIG. 2. (a) Measured spectral gain of the three-stack metal-metal QCL at selected current densities and a heat-sink temperature of 10 K. The insets show the particular operating points on the LIV curve. (b) Bias dependent gain at the center frequencies of the three quantum cascade structures. The lasing threshold of the coupled cavity device is indicated by the vertical dashed line.

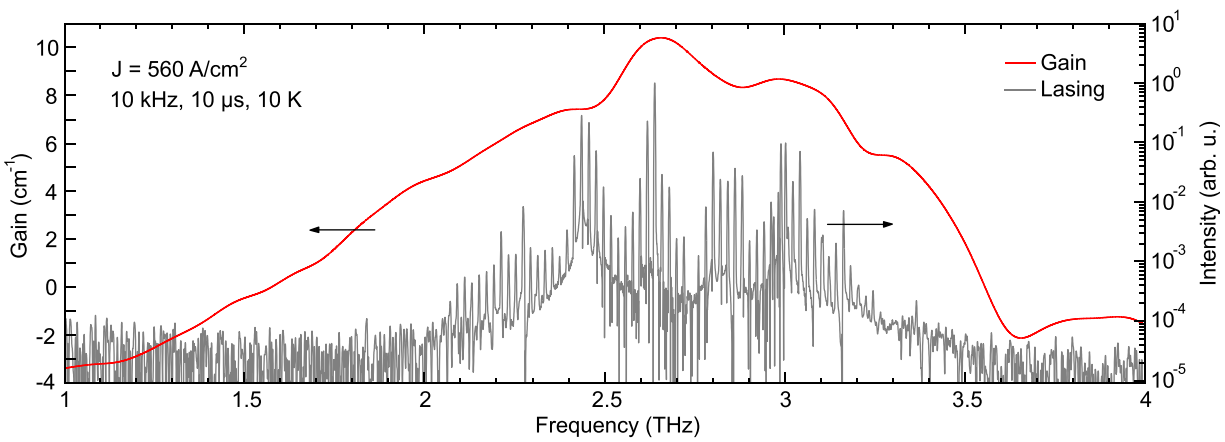


FIG. 3. Comparison of the intensity gain (THz-TDS), measured in a coupled cavity configuration, and the lasing spectrum (FTIR) of an optimized ultra-broadband THz QCL without emitter section. The active region exhibits a gain with FWHM of 1.1 THz and a lasing bandwidth of ~ 1.15 THz.

the gain reaches a value of 1.1 THz. As the current is further increased to the point of maximum QCL output power (710 A/cm^2), we observe a slight decrease of the peak gain, but contrary to the measurements on the two-stack heterogeneous active region presented in Ref. 16, we do not see a decrease of the gain FWHM with increased current densities. Figure 2(b) displays the bias dependent gain at the center frequencies of the three stacks. The gain values increase monotonically with the driving current and clamp to the frequency dependent optical losses of the laser cavity. At the threshold current density of the investigated device, indicated by the dashed vertical line in Figure 2(b), the gain at 3.0 THz is clamped to a value of 8.8 cm^{-1} . Slightly above threshold, the gain at 2.7 and 2.3 THz clamps to the value of 10.2 cm^{-1} and 7.4 cm^{-1} , respectively. The successive gain clamping of the individual active regions, correlates with the successive appearance of lasing modes centered at 3.0, 2.7, and 2.3 THz, as observed in Ref. 13. Starting from 530 A/cm^2 , the gain is fully developed and all three stacks operate simultaneously. The fact that the gain at the respective center frequencies do not saturate at identical current densities suggests different parasitic scattering between the upper laser state and the miniband for the three designs. The observed slopes in the saturation curves increase with frequency, which is in agreement with the expected increase of the upper laser state pumping efficiency for QCL active regions with higher emission energies. Furthermore, the different saturation values point out the frequency dependence of the total losses. Waveguide losses of the metal-metal resonators increase with frequency, explaining the higher clamped gain values at 2.7 and 3.0 THz compared to 2.3 THz. In addition, photons with higher emission energies are potentially reabsorbed due to intersubband transitions in stacks with lower design frequencies. We attribute the highest clamped gain value at 2.7 THz to intersubband absorption of the 2.7 THz photons in the 2.3 THz quantum cascade structure.

A comparison of the measured spectral gain and the emission spectrum of the ultra-broadband gain medium is presented in Figure 3. The lasing spectrum was measured on a single cavity metal-metal device, with similar dimensions ($2000 \times 50 \mu\text{m}$) as the coupled cavity device, and acquired

with a commercial vacuum FTIR at its maximum spectral resolution (2.25 GHz). Both THz-TDS and FTIR measurements were performed at identical operating conditions (560 A/cm^2 , 10% duty cycle), at which the quantum cascade structure exhibits the largest emission bandwidth. The maximum gain value of 10.2 cm^{-1} coincides with the spectral position of the strongest longitudinal mode at 2.65 THz, and the adjacent local maxima at 2.35 and 3.01 THz correspond to the design frequencies of the other two quantum cascade structures. The device shows a lasing bandwidth of ~ 1.15 THz within a -35 dB intensity level, ranging from 2.09 to 3.25 THz. This correlates very well with the 1.1 THz FWHM of the intensity gain, measured by THz-TDS. The spectra further indicate inhomogeneous linewidth broadening, which is obvious for an active region built from three different quantum cascade stacks. However, the gain sections are not uncoupled since they are connected through carrier injection. The moderate gain decline on the lower frequency side and the presence of continuously occurring lasing modes in this spectral region indicate the possibility of expanding the gain bandwidth by increasing the number of repetitions for the 2.3 THz active region, or by adding a fourth stack with emission below 2.3 THz. This could lead to an active region with gain bandwidth far beyond 1 THz and would pave the way towards an octave spanning THz QCL.²¹

We performed temperature dependent THz-TDS measurements to obtain information on the gain degradation at elevated operating temperatures. The QCL gain section was driven at the current density of 560 A/cm^2 , indicated by the dashed vertical line in Figure 1. Time-domain traces of the transmitted difference signal as a function of temperature are displayed in Figure 4(a). The measured pulses exhibit long lasting electric field oscillations, which arise from amplification of the THz input pulses in the spectral region with positive gain. The decrease of the amplitude and extent of these oscillations with temperature is the result of gain reduction. To rule out temperature dependent effects of the photoexcited THz generation process in the emitter section, two air-side pulses, measured at 10 and 120 K, are shown in the inset of Figure 4(a). These pulses are generated in the emitter section and are bound to the metal-air interface. They propagate

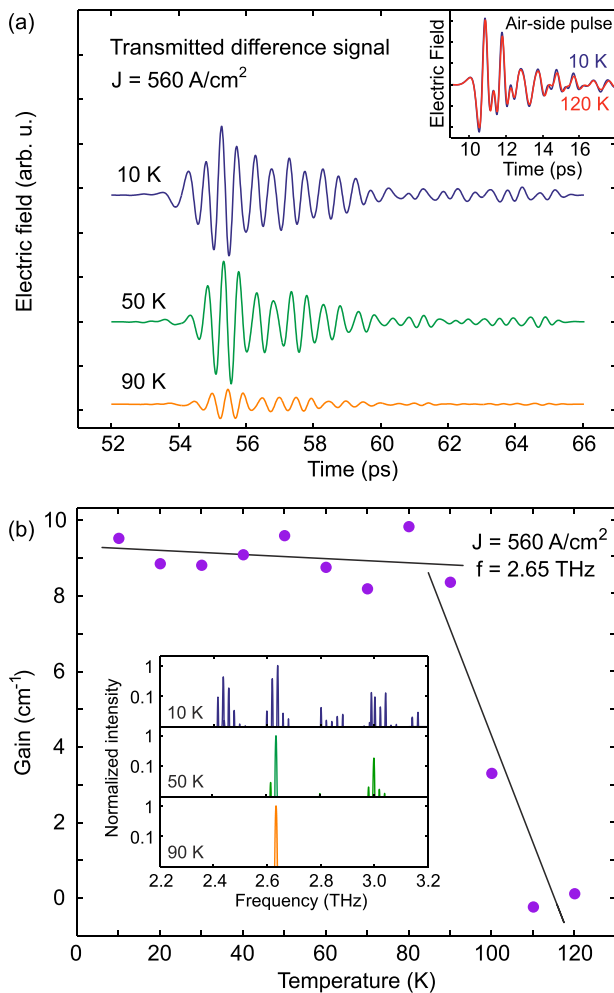


FIG. 4. Temperature dependent THz-TDS measurements. (a) Difference signal transmitted through the QCL gain section. The curves are offset for clarity. The inset shows air-side pulses at temperatures of 10 and 120 K. (b) Measured gain at 2.65 THz (dots) and linear fits of the corresponding data points (lines) for lasing and non-lasing operation. The inset displays the evolution of the lasing spectrum with temperature.

on the outer side of the metal-metal cavity, without interacting with the gain medium.¹⁷ Thus, they directly indicate the strength of the generated THz radiation. The effectively identical amplitude of the pulses at 10 and 120 K proves that the generated THz strength is not affected by the change of temperature.

Figure 4(b) displays the measured gain and the normalized emission spectrum (see inset) as a function of heat-sink temperature. As the operating temperature is increased, the intensities of the individual lasing modes are reduced, and the number of observed modes is decreased. At 90 K, just below the maximum operating temperature at the driving current density of 560 A/cm^2 , the multi-stack device exhibits single mode emission at 2.65 THz. Up to 90 K, the gain at the dominant lasing frequency of 2.65 THz is clamped to the temperature dependent optical losses of the laser cavity and slightly varies around the value of $\sim 9 \text{ cm}^{-1}$. After the laser action ceases, the measured gain rolls off sharply and reaches zero at about 110 K. Based on these observations, we conclude that the waveguide losses do not change significantly within the operating temperature range. Hence, the dominant mechanisms responsible for the gain degradation

at elevated temperatures are attributed to thermally activated LO phonon emission and reduction of the injection efficiencies into the upper laser states.^{22,23} The steep gain decline of $2.8 \text{ cm}^{-1}/10 \text{ K}$, extracted from the linear fit of the measured values between 90 and 120 K (solid line), further indicates that the maximum operating temperature of the present THz QCL device cannot be significantly improved by lowering the total optical losses of the laser cavity.

In conclusion, we have experimentally analyzed the bias and temperature dependent gain formation of a multi-stack terahertz quantum cascade laser, consisting of three different active regions, with center frequencies at 2.3, 2.7, and 3.0 THz. The bandstructure alignment of the individual quantum cascade structures occurs at slightly different driving current densities. This consequently results in a successive gain clamping and gradual initiation of laser action for the 3.0, 2.7, and 2.3 THz designs. We observe varying clamped gain values among the three stacks and attribute these to frequency dependent optical losses. Temperature dependent measurements reveal no significant change of the cavity losses within the operating temperature range and display a steep decline of the intersubband gain after laser switch off. The performance of multi-stack terahertz quantum cascade lasers, with respect to a more uniform intensity distribution between the lasing modes, might be improved by adjusting the spectral separation between the individual optical transitions, as well as the composition and the arrangement of the stacks in the metal-metal waveguide. Furthermore, the observed moderate gain decline on the lower frequency side suggests the addition of another active region below 2.3 THz, with the aim of achieving lasing bandwidths well beyond 1 THz.

The authors acknowledge partial financial support by the European Union via FET-Open grant TERACOMB ICT-296500, the Austrian Science Fund (FWF) in the Framework of the Doctoral School “Building Solids for Function” (W1243) and DK CoQus (W1210), the Austrian Nano Initiative project (PLATON), and the Austrian Society for Microelectronics (GMe).

¹X. C. Zhang and J. Xu, *Introduction to THz Wave Photonics* (Springer, New York, 2009).

²R. Köhler, A. Tredicucci, F. Beltram, H. E. Beere, E. H. Linfield, A. G. Davies, D. A. Ritchie, R. C. Iotti, and F. Rossi, *Nature* **417**, 156 (2002).

³B. S. Williams, *Nat. Photonics* **1**, 517 (2007).

⁴M. Brandstetter, C. Deutsch, M. Krall, H. Detz, D. C. MacFarland, T. Zederbauer, A. M. Andrews, W. Schrenk, G. Strasser, and K. Unterrainer, *Appl. Phys. Lett.* **103**, 171113 (2013).

⁵L. Li, L. Chen, J. Zhu, J. Freeman, P. Dean, A. Valavanis, A. G. Davies, and E. H. Linfield, *Electron. Lett.* **50**, 309 (2014).

⁶S. Fatholouloumi, E. Dupont, C. Chan, Z. Wasilewski, S. Laframboise, D. Ban, A. Mátyás, C. Jirauschek, Q. Hu, and H. C. Liu, *Opt. Express* **20**, 3866 (2012).

⁷H. W. Hübers, *IEEE J. Sel. Top. Quantum Electron.* **14**, 378 (2008).

⁸N. Jukam, S. S. Dhillon, D. Oustinov, J. Madeo, C. Manquest, S. Barbieri, C. Sirtori, S. P. Khanna, E. H. Linfield, A. G. Davies, and J. Tignon, *Nat. Photonics* **3**, 715 (2009).

⁹J. Xu, J. M. Hensley, D. B. Fenner, R. P. Green, L. Mahler, A. Tredicucci, M. G. Allen, F. Beltram, H. E. Beere, and D. A. Ritchie, *Appl. Phys. Lett.* **91**, 121104 (2007).

¹⁰S. Barbieri, M. Ravarolo, P. Gellie, G. Santarelli, C. Manquest, C. Sirtori, S. P. Khanna, E. H. Linfield, and A. G. Davies, *Nat. Photonics* **5**, 306 (2011).

- ¹¹D. Burghoff, T.-Y. Kao, N. Han, C. W. I. Chan, X. Cai, Y. Yang, D. J. Hayton, J.-R. Gao, J. L. Reno, and Q. Hu, *Nat. Photonics* **8**, 462 (2014).
- ¹²C. Gmachl, D. L. Sivco, R. Colombelli, F. Capasso, and A. Y. Cho, *Nature* **415**, 883 (2002).
- ¹³D. Turčinková, G. Scalari, F. Castellano, M. I. Amanti, M. Beck, and J. Faist, *Appl. Phys. Lett.* **99**, 191104 (2011).
- ¹⁴J. Kröll, J. Darmo, S. S. Dhillon, X. Marcadet, M. Calligaro, C. Sirtori, and K. Unterrainer, *Nature* **449**, 698 (2007).
- ¹⁵N. Jukam, S. Dhillon, Z.-Y. Zhao, G. Duerr, J. Armijo, N. Sirmons, S. Hameau, S. Barbieri, P. Filloux, C. Sirtori, X. Marcadet, and J. Tignon, *IEEE J. Sel. Top. Quantum Electron.* **14**, 436 (2008).
- ¹⁶J. R. Freeman, A. Brewer, J. Madéo, P. Cavalié, S. S. Dhillon, J. Tignon, H. E. Beere, and D. A. Ritchie, *Appl. Phys. Lett.* **99**, 241108 (2011).
- ¹⁷M. Martl, J. Darmo, C. Deutsch, M. Brandstetter, A. M. Andrews, P. Klang, G. Strasser, and K. Unterrainer, *Opt. Express* **19**, 733 (2011).
- ¹⁸D. Burghoff, T.-Y. Kao, D. Ban, A. W. M. Lee, Q. Hu, and J. Reno, *Appl. Phys. Lett.* **98**, 061112 (2011).
- ¹⁹M. I. Amanti, G. Scalari, R. Terazzi, M. Fischer, M. Beck, J. Faist, A. Rudra, P. Gallo, and E. Kapon, *New J. Phys.* **11**, 125022 (2009).
- ²⁰G. Fasching, A. Benz, K. Unterrainer, R. Zobl, A. M. Andrews, T. Roch, W. Schrenk, and G. Strasser, *Appl. Phys. Lett.* **87**, 211112 (2005).
- ²¹M. Rösch, G. Scalari, M. Beck, and J. Faist, “Octave-spanning semiconductor laser,” *Nat. Photonics* (in press).
- ²²Y. Chassagneux, Q. J. Wang, S. P. Khanna, E. Strupiechonski, J.-R. Coudeville, E. H. Linfield, A. G. Davies, F. Capasso, M. A. Belkin, and R. Colombelli, *IEEE Trans. Terahertz Sci. Technol.* **2**, 83 (2012).
- ²³M. A. Belkin, Q. J. Wang, C. Pflügl, F. Capasso, A. Belyanin, S. Khanna, A. G. Davies, and E. Linfield, *IEEE J. Sel. Top. Quantum Electron.* **15**, 952 (2009).